ACS APPLIED NANO MATERIALS
Cite This: ACS Appl. Nano Mater. 2019, 2, 667−672
Letter
www.acsanm.org

Ultrathin Graphene-Like Carbon-Coated Iron Oxide Nanocrystals for Applications in Corrosive Environments

Adriana Mendoza-Garcia,[†,‡] Caitlin M. Masterson,[†,‡] Arjun Prakash,[§] Melissa L. Nakamoto,[†] Daniel Garcia-Rojas,[§] Cigdem Ozsoy-Keskinbora,[⊥] David C. Bell,[⊥] and Vicki L. Colvin*[,†]

[†]Department of Chemistry, Brown University, Providence, Rhode Island 02912, United States
[§]Department of Chemistry, Rice University, Houston, Texas 77005, United States
[⊥]Harvard John A. Paulson School of Engineering and Applied Sciences, Harvard University, Cambridge, Massachusetts 02138, United States

Supporting Information

ABSTRACT: Here we report a solution-phase strategy for depositing ultrathin graphene-like carbon onto iron oxide nanocrystals (NCs) for corrosion resistance in magnetic and electrocatalytic applications. Thermal decomposition of iron carboxylates is a well-known method for generating uniform, size-tunable iron oxide NCs. When this reaction is completed at elevated temperatures and for longer times, the nanomaterials become unreactive to further growth and the magnetic nanomaterial survives treatment with concentrated nitric acid. X-ray photoelectron and Raman spectroscopies reveal that these materials contain graphene-like carbon. Metal carboxylates can decompose and yield carbon monoxide (CO), which we detect via gas chromatography−mass spectrometry. We speculate that when this CO is generated near a growing iron oxide surface, it disproportionates to yield carbon dioxide and carbon. Our approach is notable given that a low-temperature, solution-phase route for forming carbon materials such as graphene from the bottom up has remained elusive.

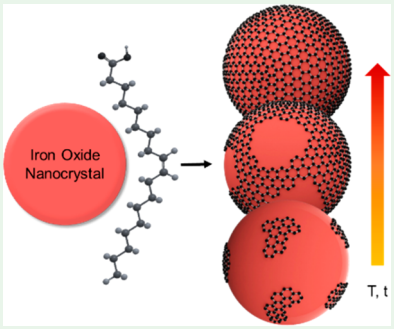

KEYWORDS: *iron oxide nanocrystals, graphene-coated, thermal decomposition, carboxylate, corrosion-resistant, magnetic, electrocatalysis*

Iron oxide nanocrystals (NCs) have valuable magnetic and chemical properties that can be applied in areas as diverse as environmental remediation, magnetic imaging, and catalysis.[1−3] Whether these materials are used in fuel cells, in the human body, or in underground aquifers, their performance depends on resistance to a wide range of temperatures and chemical conditions. For example, when introduced to the human body, nanoparticles are cleared from the blood over hours to days by phagocytic cells that dissolve particles in acidic intracellular compartments.[4,5] The subsequent release of iron leads to cellular toxicity and has limited particle applications ranging from magnetic resonance imaging to drug delivery.[6] Also, the wide range of pH and oxidative conditions found in fuel cells and aquatic environments can degrade iron oxide materials, resulting in a loss of functional properties.[7−9]

One way to enhance the nanoparticle chemical stability is to apply an inert and chemically resistant coating, such as carbon, to the particle surface. Existing methods for depositing carbon onto nanostructures rely on pyrolysis or combustion in the gas phase. These processes yield agglomerated powders covered in multilayer graphitic material that are difficult to disperse in liquids and further process.[10−13] Thicker carbon coatings can diminish the influence of metals on catalytic surfaces, as observed in carbon-coated metal catalysts, and also reduce the relaxivity and saturation magnetization of magnetic nanomaterials.[14,15]

Here we report a solution-phase strategy for depositing ultrathin graphene-like carbon onto iron oxide NCs. The process starts with thermal decomposition of iron carboxylates.[16−18] By using moderately high temperatures and longer times, the NC products become resistant to both seeded growth and Ostwald ripening. High-resolution transmission electron microscopy (HRTEM) shows crystalline iron oxide particles with no visible coating; however, both X-ray photoelectron (XPS) and Raman spectroscopies reveal significant sp^2 carbon content in dried samples. Most notably, these NCs are resistant to dissolution in concentrated nitric acid (HNO_3). This carbon coating is likely the result of carbon monoxide (CO) disproportionation at the growing iron oxide surface, a process that results in the production of both elemental carbon and carbon dioxide (CO_2).

It is well established that iron oxide NCs with highly uniform and tunable diameters result from thermal decomposition of iron carboxylates in organic solvents (Figure 1).[19−22] Iron carboxylates are formed at low temperatures

Received: January 16, 2019
Accepted: February 4, 2019
Published: February 4, 2019

DOI: 10.1021/acsanm.9b00093
ACS Appl. Nano Mater. 2019, 2, 667−672

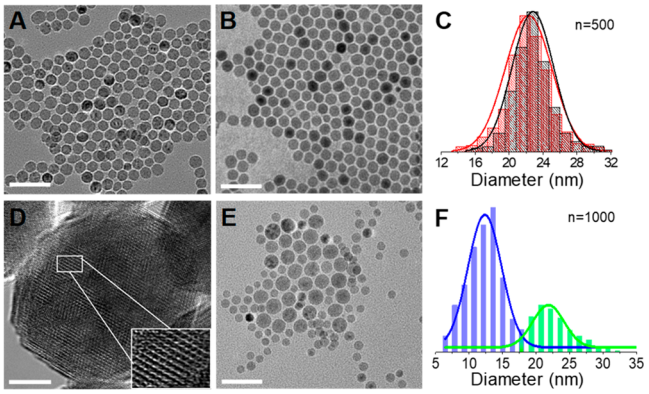

Figure 1. (A) As-synthesized NCs (final temperature 340 °C; 1 h). (B) As-synthesized NCs (final temperature 340 °C; 24 h). (C) Size distribution of NCs synthesized for 1 h (red) and 24 h (black). Neither further growth nor Ostwald ripening is observed. Here *n* refers to the number of particles measured for the graph. (D) HRTEM image of a single iron oxide crystal (340 °C, 24 h). The inset shows a zoom-in of a representative local area. The lattice fringe spacing of 0.3 nm corresponds to the interplanar spacing of (220) planes from magnetite. The scale bar is 5 nm. (E and F) Seed-mediated growth experiment showing the original population (20 nm, green) and the newly formed NCs (11 nm, blue). The scale bar is 100 nm for parts A, B, and E.

(90–200 °C) through the dissolution of an iron source, here FeOOH or $Fe(acac)_3$, by an organic acid (e.g., oleic acid). Iron carboxylate decomposition and NC formation have been reported over a range of reaction temperatures from 310 to 340 °C.[21,22] With the inclusion of oleylamine, slightly lower reaction temperatures can be adopted (e.g., 300 °C) with comparable results (Figure S1). At the very highest temperatures of 340 °C, NCs form within the first hour (Figure 1A) and exhibit little change in the dimensions or uniformity after prolonged heating (Figure 1B); no statistically significant change in their particle size distributions is observed over time (Figure 1C). HRTEM images of the NCs (Figure 1D) show lattice spacings corresponding to (220) planes of crystalline iron oxides. These microscopy data are in agreement with X-ray diffraction (XRD) of recovered powders (Figure S2), which can be indexed to magnetite (Fe_3O_4) or wüstite (FeO) in agreement with past reports.[23]

Nanoparticle dimensions also remain unchanged after the introduction of a fresh iron carboxylate precursor (Figure 1E,F). Normally, such a treatment, termed "seeded growth", leads to the growth of NCs as the molecular iron source deposits on the surfaces of the NCs.[19,24] The resistance of these NCs to conventional growth techniques suggests that their interfaces have been modified in some way to make them less reactive. Using HRTEM, the iron oxide can be clearly resolved at the atomic scale with no apparent coating (Figure S3).

Both Raman spectroscopy and XPS reveal that samples formed over 300 °C possess sp^2 carbon consistent with a graphene-like material (Figure 2). For these measurements, the black reaction product was purified via repeated sedimentation and resuspension cycles in hexanes. After purification, the NCs—and their associated surface species—were collected via magnetic separation (Figure S4). The NCs formed at elevated temperatures have Raman peaks consistent with those of carbon allotropes containing substantial sp^2 content (Figure

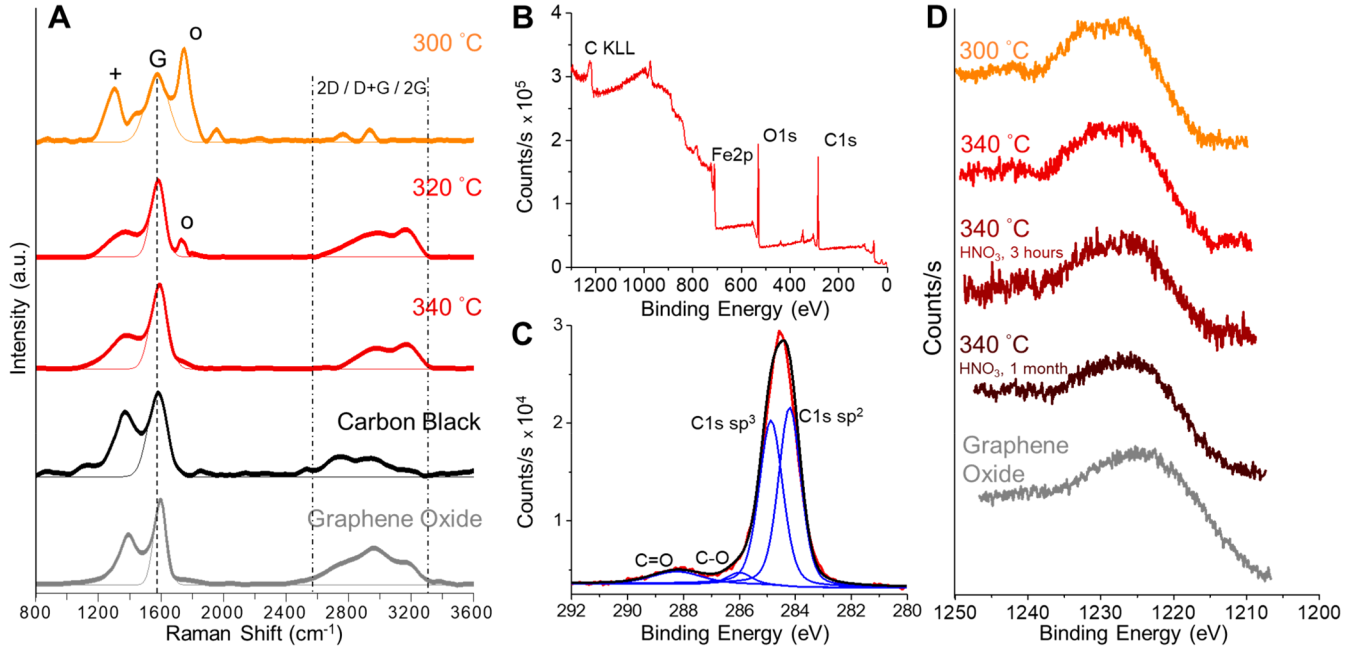

Figure 2. (A) Raman spectra for iron oxide NCs synthesized at different temperatures for 24 h. Spectra of commercial carbon black and graphene oxide are presented as references. A 405 nm laser source was used to avoid fluorescence and iron oxide oxidation. All spectra were normalized with respect to the intensity of the G band (dash line), for which the position and width were modeled to estimate the sp^2 content (Figure S7). The region enclosed by the dash-dotted lines shows the higher-order peaks (2D, D + G, and 2G). Oleate-related peaks are identified with an "o" sign, while iron oxide related peaks are identified with a + sign. (B) XPS survey scan of iron oxide NCs synthesized at 340 °C for 24 h. The Fe 2p, O 1s, and C 1s and Auger KLL carbon peaks are highlighted. (C) C 1s XPS peak of NCs synthesized at 340 °C for 24 h showing the fractions of carbon (see the Supporting Information). (D) Auger KLL carbon peaks of iron oxide NCs before and after acid treatment. The derivative of this peak is used to define the *D* parameter, which is a measure of the sp^2 carbon content. The graphene oxide standard is shown as a reference.

DOI: 10.1021/acsanm.9b00093
ACS Appl. Nano Mater. 2019, 2, 667–672

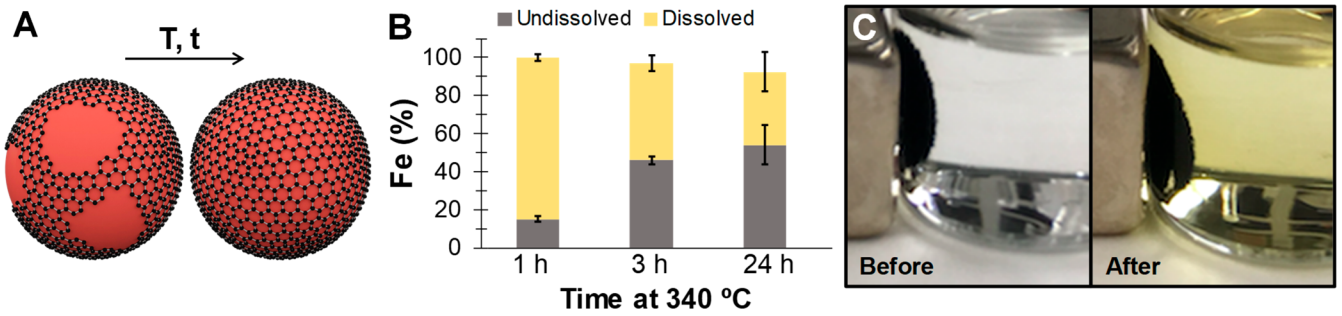

Figure 3. (A) Schematic illustrating a partial surface coating of graphitic carbon and a more complete graphene shell around NCs. (B) Iron (w/w %) leached after exposure of NCs to a 50% HNO_3 solution for 3 h (yellow). The amount of iron that remains as NCs (gray) is also presented. NCs were synthesized at 340 °C for 1, 3, and 24 h. While a large portion of the NCs dissolve for the sample heated for 1 h, slightly more than half dissolve when the synthesis time is increased to 3 h, and less than half dissolve when the reaction time is increased to 24 h. (C) NCs before and after acid treatment. The samples retain their magnetic properties.

2A).[25−27] A strong band located at ∼1580 cm^{-1} corresponds to the graphite G band.[25] Also found in these NCs is the D band at 1350 cm^{-1} associated with disorder in graphitic materials.[26] Complicating any quantitative analysis of this peak, however, is the presence of a 1310 cm^{-1} iron oxide band; this feature is more pronounced at excitation wavelengths of 532 nm (Figure S5).[28,29] The 2D band located at ∼2600 cm^{-1} and other higher-order peaks were not interpreted here because their intensity and position were influenced by the substrate, strain, and morphology.[30] Analysis of the G bandwidth and position relative to various carbon standards shows that NCs have spectroscopic features most similar to those of graphene (Figure S6). In general, higher reaction temperatures and longer times yielded a narrower G band, suggesting the formation of more ordered regions of sp^2 carbon.[31]

XPS confirms the presence of sp^2 carbon in our samples (Figure 2B−D). The full spectrum (Figures 2B and S7) identifies iron, carbon, and oxygen associated with the NCs. Figure 2D shows in detail the C 1s peak for a sample heated at 340 °C for 24 h. Quantitative analysis of carbon speciation from C 1s peak fits is challenging even in pure samples.[32,33] Significant sp^3 carbon features are typical in many graphene and NC samples because of the contribution of adventitious carbon and residual surfactant (Figure 2C).[34] A more reliable method for assessing the content of sp^2 carbon uses the width of the derivative of the Auger KLL carbon peak (Figure 2D), referred to as the *D* parameter (Figure S8).[35−37] This parameter provides a more precise measure of the relative sp^2 content and has been validated for many known carbon standards.[38−41] Using this approach, we find 40% of the carbon in the NC samples has sp^2 character; for comparison, a carbon nanotube sample is typically 50% sp^2, while our graphene oxide standard is 60% sp^2 (Figure S9). Moreover, the content of sp^2 carbon as measured by the *D* parameter increases with higher reaction temperatures and the removal of surface-bound carboxylates, consistent with our observations from Raman spectroscopy.

Because magnetic separation was used to collect these NCs, the carbon features identified in Figure 2 must be surface associated with the iron oxide NCs. To determine how thick of a coating might be present, we applied quantitative elemental analysis (Table S1). The NC samples contained very small amounts of carbon (<15 w/w %). This is consistent with the magnetization data, which find that the materials have saturation values close to bulk magnetite (Figure S4), indicating that the sample mass is mostly magnetic material.[42] Elemental analysis is agnostic as to the source of carbon: some will be the sp^2 carbon detected by XPS and Raman spectroscopy (Figure 2), while the remainder is the residual organic carbon also observed in these spectroscopies. If we make the extreme assumption that all of the carbon is sp^2, we would estimate that the coatings are at most one to two monolayers of carbon. Within a NC sample, we could have some particles coated with patchy graphitic surfaces as well as some with a complete graphene-like shell (Figure 3A).

HRTEM images of these particles (Figure S9) cannot clearly resolve monolayer carbon on a higher-contrast material like iron oxide. Imaging of carbon at the interface of higher-contrast materials has only been demonstrated for multiple layers of carbon.[43] In this case, multiple layers cannot be generated because the carbon production process requires active iron oxide surfaces. Further complicating the application of tools such as High-angle annular dark-field scanning transmission electron microscopy is the presence of residual organic carbon in samples. This leads to charging of the samples and loss of the near-angstrom resolution required to resolve carbon atoms at the surface of iron oxide.[44,45] In the absence of direct imaging evidence for the structures proposed in Figure 3A, we turned toward more functional analysis of the materials.

We reasoned that the chemical properties of the NCs, particularly their resistance to acid dissolution, would provide the best insight into the extent of the carbon coating. Bulk iron oxide dissolves instantaneously in concentrated HNO_3;[46] we verified that this is also true for nanoparticles made with this synthesis at lower temperatures (Figure S10). In contrast, the NC samples produced at higher temperatures did not fully dissolve under the same conditions: over 50% of the magnetic material survived treatment with acid (Figure 3B,C and Video S1). This drastic change in the chemical properties between low- and high-temperature heating indicates that the particle interfaces have undergone substantial alteration.

One hallmark of a graphitic coating is its ability to render underlying materials chemically resistant. This observation, along with our spectroscopic evidence in Figure 2, led us to the conclusion that our iron oxide NCs can become completely coated with graphene-like shells. Graphene coatings are well-known to provide chemical resistance to a wide range of metals and metal oxides. In one case, chemical vapor deposition of graphene yielded metals that resisted oxidation;[47] additionally, carbon coating of electrocatalysts is motivated, in part, by protecting materials like iron oxide from harsh, acidic

DOI: 10.1021/acsanm.9b00093
ACS Appl. Nano Mater. 2019, 2, 667−672

conditions.[8,15] The process described here does not produce 100% yield of fully coated materials; some material does dissolve quickly, and we attribute this to the presence of patchy, incomplete coatings (Figure 3A, left). However, after 24 h of heating, more than half of the sample mass remains after acid treatment. Analysis of this persistent, magnetic fraction by Raman, XPS, and XRD reveals iron and carbon species similar to the original material (Figures 2D and S11). A notable shift is in the appearance of oxidized carbon; other sp^2 carbon allotropes oxidize when treated with concentrated HNO_3.[48,49] Because the extent of oxidation could not be known, morphological characterizations were not performed after acid treatment. The data suggest that the yield of fully coated NCs increases with prolonged heating, as illustrated by the increasing mass of acid-resistant material in samples heated the longest (Figure 3B). Patches of graphitic carbon may develop early in the reaction and over time form into complete shells (Figure 3A, right).

The generation of elemental carbon during the formation of NCs was unexpected, and we analyzed the gas-phase products evolved during the reaction to characterize the mechanism (Figure 4A). Both CO and CO_2 are reported byproducts of

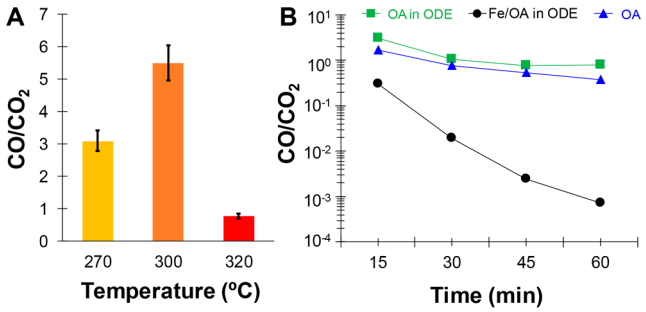

Figure 4. Ratio of CO/CO_2 evolved (A) with the reaction temperature and (B) against time at 320 °C, as computed from gas chromatography–mass spectrometry. During heating at 320 °C, the ratio of CO/CO_2 that evolved during particle synthesis differs by 2 orders of magnitude compared with the heating of only oleic acid (OA) or a mixture of oleic acid and octadecene (OA in ODE), suggesting the utilization of CO and its conversion to CO_2 in the presence of iron.

thermal decomposition of iron oleate in organic media.[17,50] When the reaction is kept at temperatures over 300 °C, we initially observe higher levels of CO; these levels decline as more CO_2 is detected with time (Figure 4B). In the absence of iron, the decomposition process yields predominantly CO; when iron is present, significantly greater levels of CO_2 are observed. CO is well known to disproportionate at iron/iron oxide surfaces through the Boudouard reaction:[51,52]

$$2CO \rightarrow CO_2 + C$$

Our data suggest that if disproportionation occurs, it is less favored at shorter reaction times or lower temperatures, and particle surfaces remain unchanged. Conversely, at longer times and higher temperatures, graphitic carbon is generated in greater quantity and may completely encase the particles. CO_2 is also generated through the direct reduction of iron oxide by CO, which is observed by XRD (Figure S2); however, the presence of enough elemental carbon to coat the NCs suggests that the contribution of the disproportionation reaction to the total CO_2 is probably predominant. The proposed mechanism could also explain why such thin coatings are observed: once carbon forms and deposits on the particle surface, it blocks further disproportionation.

The generation of graphitic carbon by metal oxides, in particular iron-based catalysts, has been observed before by different communities.[52−54] Metal oxide catalysts are used to reform biofuels at temperatures as low as 400 °C; typically granular and non-nanoscale, these materials will reduce the fatty acid content in feedstocks but can become poisoned by carbon deposition at their interfaces.[54] These researchers have proposed a mechanism similar to that described here to explain their observations.[52]

In summary, the process of iron carboxylate decomposition at temperatures over 300 °C can lead to the formation of graphene-like carbon at the surface of iron oxide NCs. Both XPS and Raman spectroscopy indicate that the surface-associated carbon resembles a graphene material. Only small amounts of carbon are found in the NC samples, suggesting that these coatings may be patchy at early times and, even when fully formed, do not contain more than one or two monolayers of carbon. The decomposition of carboxylates at high temperatures can yield CO, a gas-phase species the we detect in the absence of iron. We propose that, in the presence of iron oxide, CO disproportionates into CO_2 and elemental carbon, which deposits onto the surfaces of the NCs. Even though the carbon coatings are too thin to be definitively resolved by electron microscopy, their existence is revealed by spectroscopy. Most notably, the presence of complete graphene-like coatings is the only explanation for the remarkable acid resistance of the materials. These observations suggest a starting point for forming graphene and nanostructured carbon at temperatures below 400 °C in a solution-phase environment.

■ ASSOCIATED CONTENT

Supporting Information

The Supporting Information is available free of charge on the ACS Publications website at DOI: 10.1021/acsanm.9b00093.

Materials, experimental methods, and supplementary figures and tables (PDF)

Video of a NC sample produced at higher temperature that did not fully dissolve (MPG)

■ AUTHOR INFORMATION

Corresponding Author

*E-mail: vicki_colvin@brown.edu.

ORCID

Adriana Mendoza-Garcia: 0000-0002-2892-4470

Caitlin M. Masterson: 0000-0003-4264-6291

Melissa L. Nakamoto: 0000-0003-0955-6710

Daniel Garcia-Rojas: 0000-0002-6462-4205

Cigdem Ozsoy-Keskinbora: 0000-0002-3059-0852

Vicki L. Colvin: 0000-0002-8526-515X

Author Contributions

‡These authors contributed equally.

Notes

The authors declare no competing financial interest.

■ ACKNOWLEDGMENTS

This work was performed, in part, at the Harvard University Center for Nanoscale Systems, a member of the National

DOI: 10.1021/acsanm.9b00093
ACS Appl. Nano Mater. 2019, 2, 667−672

Nanotechnology Coordinated Infrastructure Network, which is supported by the National Science Foundation (NSF) under NSF ECCS Award 1541959. C.O.-K. and D.C.B. acknowledge support by the Center for Integrated Quantum Materials under NSF Grant DMR-1231319. The authors thank Dr. Greg Lin for assistance with XPS measurements and Muchun Liu for providing the graphene oxide sample.

REFERENCES

(1) Lee, N.; Yoo, D.; Ling, D.; Cho, M. H.; Hyeon, T.; Cheon, J. Iron Oxide Based Nanoparticles for Multimodal Imaging and Magnetoresponsive Therapy. *Chem. Rev.* **2015**, *115*, 10637−10689.
(2) Xu, P. A.; Zeng, G. M.; Huang, D. L.; Feng, C. L.; Hu, S.; Zhao, M. H.; Lai, C.; Wei, Z.; Huang, C.; Xie, G. X.; Liu, Z. F. Use of Iron Oxide Nanomaterials in Wastewater Treatment: A Review. *Sci. Total Environ.* **2012**, *424*, 1−10.
(3) Shylesh, S.; Schunemann, V.; Thiel, W. R. Magnetically Separable Nanocatalysts: Bridges between Homogeneous and Heterogeneous Catalysis. *Angew. Chem., Int. Ed.* **2010**, *49*, 3428−3459.
(4) Gustafson, H. H.; Holt-Casper, D.; Grainger, D. W.; Ghandehari, H. Nanoparticle Uptake: The Phagocyte Problem. *Nano Today* **2015**, *10*, 487−510.
(5) Petri-Fink, A.; Steitz, B.; Finka, A.; Salaklang, J.; Hofmann, H. Effect of Cell Media on Polymer Coated Superparamagnetic Iron Oxide Nanoparticles (SPIONs): Colloidal Stability, Cytotoxicity, and Cellular Uptake Studies. *Eur. J. Pharm. Biopharm.* **2008**, *68*, 129−137.
(6) Arbab, A. S.; Wilson, L. B.; Ashari, P.; Jordan, E. K.; Lewis, B. K.; Frank, J. A. A Model of Lysosomal Metabolism of Dextran Coated Superparamagnetic Iron Oxide (SPIO) Nanoparticles: Implications for Cellular Magnetic Resonance Imaging. *NMR Biomed.* **2005**, *18*, 383−389.
(7) Lei, C.; Sun, Y. Q.; Tsang, D. C. W.; Lin, D. H. Environmental Transformations and Ecological Effects of Iron-Based Nanoparticles. *Environ. Pollut.* **2018**, *232*, 10−30.
(8) Deng, J.; Ren, P. J.; Deng, D. H.; Bao, X. H. Enhanced Electron Penetration through an Ultrathin Graphene Layer for Highly Efficient Catalysis of the Hydrogen Evolution Reaction. *Angew. Chem., Int. Ed.* **2015**, *54*, 2100−2104.
(9) Baalousha, M.; Manciulea, A.; Cumberland, S.; Kendall, K.; Lead, J. R. Aggregation and Surface Properties of Iron Oxide Nanoparticles: Influence of pH and Natural Organic Matter. *Environ. Toxicol. Chem.* **2008**, *27*, 1875−1882.
(10) Seo, W. S.; Lee, J. H.; Sun, X. M.; Suzuki, Y.; Mann, D.; Liu, Z.; Terashima, M.; Yang, P. C.; McConnell, M. V.; Nishimura, D. G.; Dai, H. J. FeCo/Graphitic-Shell Nanocrystals as Advanced Magnetic-Resonance-Imaging and Near-Infrared Agents. *Nat. Mater.* **2006**, *5*, 971−976.
(11) Chen, Z.; Hong, G. S.; Wang, H. L.; Welsher, K.; Tabakman, S. M.; Sherlock, S. P.; Robinson, J. T.; Liang, Y. Y.; Dai, H. J. Graphite-Coated Magnetic Nanoparticle Microarray for Few-Cells Enrichment and Detection. *ACS Nano* **2012**, *6*, 1094−1101.
(12) Lee, S. J.; Cho, J. H.; Lee, C.; Cho, J.; Kim, Y. R.; Park, J. K. Synthesis of Highly Magnetic Graphite-Encapsulated FeCo Nanoparticles Using a Hydrothermal Process. *Nanotechnology* **2011**, *22*, 375603.
(13) Park, J. K.; Jung, J.; Subramaniam, P.; Shah, B. P.; Kim, C.; Lee, J. K.; Cho, J. H.; Lee, C.; Lee, K. B. Graphite-Coated Magnetic Nanoparticles as Multimodal Imaging Probes and Cooperative Therapeutic Agents for Tumor Cells. *Small* **2011**, *7*, 1647−1652.
(14) Host, J. J.; Block, J. A.; Parvin, K.; Dravid, V. P.; Alpers, J. L.; Sezen, T.; LaDuca, R. Effect of Annealing on the Structure and Magnetic Properties of Graphite Encapsulated Nickel and Cobalt Nanocrystals. *J. Appl. Phys.* **1998**, *83*, 793−801.
(15) Deng, D. H.; Yu, L.; Chen, X. Q.; Wang, G. X.; Jin, L.; Pan, X. L.; Deng, J.; Sun, G. Q.; Bao, X. H. Iron Encapsulated within Pod-like Carbon Nanotubes for Oxygen Reduction Reaction. *Angew. Chem., Int. Ed.* **2013**, *52*, 371−375.
(16) Kemp, S. J.; Ferguson, R. M.; Khandhar, A. P.; Krishnan, K. M. Monodisperse Magnetite Nanoparticles with Nearly Ideal Saturation Magnetization. *RSC Adv.* **2016**, *6*, 77452−77464.
(17) Kwon, S. G.; Piao, Y.; Park, J.; Angappane, S.; Jo, Y.; Hwang, N. M.; Park, J. G.; Hyeon, T. Kinetics of Monodisperse Iron Oxide Nanocrystal Formation by "Heating-Up" Process. *J. Am. Chem. Soc.* **2007**, *129*, 12571−12584.
(18) Bronstein, L. M.; Huang, X. L.; Retrum, J.; Schmucker, A.; Pink, M.; Stein, B. D.; Dragnea, B. Influence of Iron Oleate Complex Structure on Iron Oxide Nanoparticle Formation. *Chem. Mater.* **2007**, *19*, 3624−3632.
(19) Sun, S.; Zeng, H. Size-Controlled Synthesis of Magnetite Nanoparticles. *J. Am. Chem. Soc.* **2002**, *124*, 8204−8205.
(20) Tromsdorf, U. I.; Bruns, O. T.; Salmen, S. C.; Beisiegel, U.; Weller, H. A Highly Effective, Nontoxic T-1 MR Contrast Agent Based on Ultrasmall PEGylated Iron Oxide Nanoparticles. *Nano Lett.* **2009**, *9*, 4434−4440.
(21) Park, J.; An, K. J.; Hwang, Y. S.; Park, J. G.; Noh, H. J.; Kim, J. Y.; Park, J. H.; Hwang, N. M.; Hyeon, T. Ultra-Large-Scale Syntheses of Monodisperse Nanocrystals. *Nat. Mater.* **2004**, *3*, 891−895.
(22) Yu, W. W.; Falkner, J. C.; Yavuz, C. T.; Colvin, V. L. Synthesis of Monodisperse Iron Oxide Nanocrystals by Thermal Decomposition of Iron Carboxylate Salts. *Chem. Commun.* **2004**, 2306−2307.
(23) Redl, F. X.; Black, C. T.; Papaefthymiou, G. C.; Sandstrom, R. L.; Yin, M.; Zeng, H.; Murray, C. B.; O'Brien, S. P. Magnetic, Electronic, and Structural Characterization of Nonstoichiometric Iron Oxides at the Nanoscale. *J. Am. Chem. Soc.* **2004**, *126*, 14583−14599.
(24) Park, J.; Lee, E.; Hwang, N. M.; Kang, M. S.; Kim, S. C.; Hwang, Y.; Park, J. G.; Noh, H. J.; Kim, J. Y.; Park, J. H.; Hyeon, T. One-Nanometer-Scale Size-Controlled Synthesis of Monodisperse Magnetic Iron Oxide Nanoparticles. *Angew. Chem., Int. Ed.* **2005**, *44*, 2872−2877.
(25) Ferrari, A. C.; Robertson, J. Interpretation of Raman Spectra of Disordered and Amorphous Carbon. *Phys. Rev. B: Condens. Matter Mater. Phys.* **2000**, *61*, 14095−14107.
(26) Dresselhaus, M. S.; Dresselhaus, G.; Saito, R.; Jorio, A. Raman Spectroscopy of Carbon Nanotubes. *Phys. Rep.* **2005**, *409*, 47−99.
(27) Gupta, S.; Saxena, A. Nanocarbon Materials: Probing the Curvature and Topology Effects Using Phonon Spectra. *J. Raman Spectrosc.* **2009**, *40*, 1127−1137.
(28) Butler, H. J.; Ashton, L.; Bird, B.; Cinque, G.; Curtis, K.; Dorney, J.; Esmonde-White, K.; Fullwood, N. J.; Gardner, B.; Martin-Hirsch, P. L.; Walsh, M. J.; McAinsh, M. R.; Stone, N.; Martin, F. L. Using Raman Spectroscopy to Characterize Biological Materials. *Nat. Protoc.* **2016**, *11*, 664−687.
(29) El Mendili, Y.; Bardeau, J. F.; Randrianantoandro, N.; Gourbil, A.; Greneche, J. M.; Mercier, A. M.; Grasset, F. New Evidences of in Situ Laser Irradiation Effects on γ-Fe_2O_3 Nanoparticles: A Raman Spectroscopic Study. *J. Raman Spectrosc.* **2011**, *42*, 239−242.
(30) Saito, R.; Hofmann, M.; Dresselhaus, G.; Jorio, A.; Dresselhaus, M. S. Raman Spectroscopy of Graphene and Carbon Nanotubes. *Adv. Phys.* **2011**, *60*, 413−550.
(31) Tomasini, E. P.; Halac, E. B.; Reinoso, M.; Di Liscia, E. J.; Maier, M. S. Micro-Raman Spectroscopy of Carbon-Based Black Pigments. *J. Raman Spectrosc.* **2012**, *43*, 1671−1675.
(32) Ferro, S.; Dal Colle, M.; De Battisti, A. Chemical Surface Characterization of Electrochemically and Thermally Oxidized Boron-Doped Diamond Film Electrodes. *Carbon* **2005**, *43*, 1191−1203.
(33) Singh, B.; Diwan, A.; Jain, V.; Herrera-Gomez, A.; Terry, J.; Linford, M. R. Uniqueness Plots: A Simple Graphical Tool for Identifying Poor Peak Fits in X-ray Photoelectron Spectroscopy. *Appl. Surf. Sci.* **2016**, *387*, 155−162.
(34) Evans, S. Correction for the Effects of Adventitious Carbon Overlayers in Quantitative XPS Analysis. *Surf. Interface Anal.* **1997**, *25*, 924−930.
(35) Lascovich, J. C.; Giorgi, R.; Scaglione, S. Evaluation of the sp^2/sp^3 Ratio in Amorphous Carbon Structure by XPS and XAES. *Appl. Surf. Sci.* **1991**, *47*, 17−21.

DOI: 10.1021/acsanm.9b00093
ACS Appl. Nano Mater. 2019, 2, 667−672

(36) Jackson, S. T.; Nuzzo, R. G. Determining Hybridization Differences for Amorphous Carbon from the XPS C 1s Envelope. *Appl. Surf. Sci.* **1995**, *90*, 195−203.
(37) Mizokawa, Y.; Miyasato, T.; Nakamura, S.; Geib, K. M.; Wilmsen, C. W. Comparison of the CKLL 1st-Derivative Auger Spectra from XPS and AES Using Diamond, Graphite, SiC and Diamond-Like-Carbon Films. *Surf. Sci.* **1987**, *182*, 431−438.
(38) Merel, P.; Tabbal, M.; Chaker, M.; Moisa, S.; Margot, J. Direct Evaluation of the sp^3 Content in Diamond-Like-Carbon Films by XPS. *Appl. Surf. Sci.* **1998**, *136*, 105−110.
(39) Mezzi, A.; Kaciulis, S. Surface Investigation of Carbon Films: From Diamond to Graphite. *Surf. Interface Anal.* **2010**, *42*, 1082−1084.
(40) Kaciulis, S. Spectroscopy of Carbon: From Diamond to Nitride Films. *Surf. Interface Anal.* **2012**, *44*, 1155−1161.
(41) Lesiak, B.; Kover, L.; Toth, J.; Zemek, J.; Jiricek, P.; Kromka, A.; Rangam, N. C sp^2 /sp^3 Hybridisations in Carbon Nanomaterials - XPS and (X)AES Study. *Appl. Surf. Sci.* **2018**, *452*, 223−231.
(42) Mendoza-Garcia, A.; Sun, S. Recent Advances in the High-Temperature Chemical Synthesis of Magnetic Nanoparticles. *Adv. Funct. Mater.* **2016**, *26*, 3809−3817.
(43) Mendes, R. G.; Bachmatiuk, A.; El-Gendy, A. A.; Melkhanova, S.; Klingeler, R.; Buchner, B.; Rummeli, M. H. A Facile Route to Coat Iron Oxide Nanoparticles with Few-Layer Graphene. *J. Phys. Chem. C* **2012**, *116*, 23749−23756.
(44) Banhart, F. Interactions between Metals and Carbon Nanotubes: At the Interface between Old and New Materials. *Nanoscale* **2009**, *1*, 201−213.
(45) Zhang, X. F.; Yan, Q. G.; Li, J. H.; Chu, I. W.; Toghiani, H.; Cai, Z. Y.; Zhang, J. L. Carbon-Based Nanomaterials from Biopolymer Lignin via Catalytic Thermal Treatment at 700 to 1000 °C. *Polymers* **2018**, *10*, 183.
(46) Salmimies, R.; Mannila, M.; Kallas, J.; Hakkinen, A. Acidic Dissolution of Magnetite: Experimental Study on the Effects of Acid Concentration and Temperature. *Clays Clay Miner.* **2011**, *59*, 136−146.
(47) Chen, S. S.; Brown, L.; Levendorf, M.; Cai, W. W.; Ju, S. Y.; Edgeworth, J.; Li, X. S.; Magnuson, C. W.; Velamakanni, A.; Piner, R. D.; Kang, J. Y.; Park, J.; Ruoff, R. S. Oxidation Resistance of Graphene-Coated Cu and Cu/Ni Alloy. *ACS Nano* **2011**, *5*, 1321−1327.
(48) Lakshminarayanan, P. V.; Toghiani, H.; Pittman, C. U. Nitric Acid Oxidation of Vapor Grown Carbon Nanofibers. *Carbon* **2004**, *42*, 2433−2442.
(49) Zhang, N.; Wang, L. Y.; Liu, H.; Cai, Q. K. Nitric Acid Oxidation on Carbon Dispersion and Suspension Stability. *Surf. Interface Anal.* **2008**, *40*, 1190−1194.
(50) Kim, D.; Park, J.; An, K.; Yang, N. K.; Park, J. G.; Hyeon, T. Synthesis of Hollow Iron Nanoframes. *J. Am. Chem. Soc.* **2007**, *129*, 5812−5813.
(51) Li, P.; Miser, D. E.; Rabiei, S.; Yadav, R. T.; Hajaligol, M. R. The Removal of Carbon Monoxide by Iron Oxide Nanoparticles. *Appl. Catal., B* **2003**, *43*, 151−162.
(52) Turkdogan, E. T.; Vinters, J. V. Catalytic Effect of Iron on Decomposition of Carbon Monoxide: 1. Carbon Deposition in H_2-CO Mixtures. *Metall. Trans.* **1974**, *5*, 11−19.
(53) Walker, P. L.; Rakszawski, J. F.; Imperial, G. R. Carbon Formation from Carbon Monoxide-Hydrogen Mixtures over Iron Catalysts. 2. Rates of Carbon Formation. *J. Phys. Chem.* **1959**, *63*, 140−149.
(54) Zeng, Z.; Natesan, K.; Maroni, V. A. Investigation of Metal-Dusting Mechanism in Fe-Base Alloys Using Raman Spectroscopy, X-ray Diffraction, and Electron Microscopy. *Oxid. Met.* **2002**, *58*, 147−170.

DOI: 10.1021/acsanm.9b00093
ACS Appl. Nano Mater. 2019, 2, 667−672